

Electron excitation rate in dielectrics under an intense elliptically polarized laser field

Prachi Venkat* and Tomohito Otake†

Kansai Photon Science Institute, National Institutes for Quantum Science and Technology (QST), Kizugawa, Kyoto 619-0215, Japan

Electron excitation in dielectrics is studied for an elliptically polarized laser field. As the first step, we develop an analytical formula for electron excitation rate under elliptically polarized laser as the extension of our previous work [T. Otake *et al.*, JPSJ **88** (2019) 024709]. In the next step, we calculate the excitation rate depending on the band structure by assuming direction dependence of reduced mass. We find that although the ellipticity decreases the excitation rate significantly in an isotropic system, the energy oscillation of electrons due to the intra-band dynamics in the anisotropic band structure increases the excitation rate with higher ellipticity. Our results indicate that we can control the excitation rate in dielectrics by varying the ellipticity, depending on the band anisotropy.

1. Introduction

Electron excitation in dielectrics by an intense laser field is the main process in laser-matter interactions. Technical developments in femtosecond laser processing have made it possible to produce a nano-scale laser-induced periodic surface structure (LIPSS),^{1–4)} and to realize non-thermal ablation for sub-wavelength resolution. In particular, for femtosecond lasers, electron excitation by multi-photon absorption and tunneling process is crucial because such non-linear processes generate a controllable free-carrier density and confine material change to the focal volume. Therefore, the prediction of electron excitation rate using theoretical models and/or numerical simulation is important. Non-linear carrier dynamics finds application in various fields of laser-matter interaction such as HHG,^{5,6)} transient transmission changes the carrier-envelope-phase-dependent electronic currents.⁷⁾

Electron excitation can be carried out by various mechanisms such as multi-photon absorption and tunneling, depending on the laser parameters. Various models have been proposed over the years to model multi-photon processes and tunneling of electrons numerically. The Keldysh theory describes electron excitation in atoms and crystals,^{8,9)} and various mechanisms have been developed based on the Keldysh approach.^{10–15)}

Incident laser intensity is a paramount factor in deciding whether the interaction follows linear or non-linear dynamics. Similarly, the polarization of the incident laser field significantly affects the carrier excitation process and optical properties of a material. The time-resolved dynamic Franz–Keldysh effect, which is responsible for the change in the dielectric function of target material, depends significantly on the polarization of incident field.¹⁶⁾

Change in the polarization of laser field also affects the dynamic phase of electrons undergoing intra-band motion, ultimately affecting the excitation rate during multi-photon absorption. For example, circularly polarized lasers are also important as an ultrafast laser waveguides,¹⁷⁾ and in controlling laser-induced nonstructure.¹⁸⁾ M. Kozák *et al.* have reported that the ellipticity of the laser polarization decreases the exci-

tation rate in diamond.¹⁹⁾ On the other hand, V. V. Temnov *et al.* have reported that the electron excitation rate induced by a circularly polarized laser is twice that induced by a linearly polarized laser at the same laser irradiance in fused silica and sapphire.²⁰⁾ We have to study the laser-matter interaction with elliptically polarized laser in order to understand the above two conflicting experiments.

The electron excitation dynamics has been numerically studied, employing the time-dependent density functional theory (TDDFT)^{21–23)} as well as analytical models.^{15,24)} Although the numerical simulation employing TDDFT is one of the most accurate approaches, it needs a sizeable computational resource, and analyzing the details of the physical process is sometimes demanding. The analytical approach is not accurate like TDDFT, although we can use it to study the physics of the interaction in detail.

In this paper, we adopt an analytical approach to obtain the electron excitation rate for the interaction of isotropic dielectrics with an intense elliptically polarized laser field. The formulation is based on the general formula presented in the previous study.¹⁵⁾ The effect of ellipticity of incident laser field on excitation rate is also studied. Furthermore, we study the dominance of n -order photonic processes at different intensities for elliptical polarization. We also extended the fundamental equation to the anisotropic band by assuming the direction-dependent reduced mass. We performed real-time simulations for carrier density after the laser pulse ends and analyzed the effect of anisotropy of the system.

This paper is organized as follows: Section 2 describes the analytical formulation of the excitation rate for elliptically polarized field with isotropic and anisotropic band structures, section 3 presents results of electron excitation in a diamond for different laser and material parameters, and then finally, we would like to summarize the work in section 4.

2. Formulation

Starting with the Schrödinger equation which is assumed as,

$$\epsilon_{n,\mathbf{k}}^G u_{n,\mathbf{k}}^G(\mathbf{r}) = \left(\frac{1}{2m} (\mathbf{p} + \hbar\mathbf{k})^2 + V(\mathbf{r}) \right) u_{n,\mathbf{k}}^G(\mathbf{r}) \quad (1)$$

\mathbf{p} being the momentum operator and \mathbf{k} being the Bloch wave vector. $V(\mathbf{r})$ is the potential and $\epsilon_{n,\mathbf{k}}^G$ and $u_{n,\mathbf{k}}^G(\mathbf{r})$ are the energy and wave functions, respectively, corresponding to the \mathbf{k} and n^{th} band. Both $V(\mathbf{r})$ and $u_{n,\mathbf{k}}^G(\mathbf{r})$ are periodic in space. The time-dependent Schrödinger equation is described as

$$\left[\frac{1}{2m} \left(\mathbf{p} + \hbar \mathbf{k} + \frac{e}{\hbar c} \mathbf{A}(t) \right)^2 + V(\mathbf{r}) \right] u_{n,\mathbf{k}}(\mathbf{r}, t) = i\hbar \frac{\partial}{\partial t} u_{n,\mathbf{k}}(\mathbf{r}, t), \quad (2)$$

where $\mathbf{A}(t)$ is the vector potential for an elliptically polarized field:²⁵⁾

$$\vec{A}(t) = A_0(\eta \sin(\omega t), 0, \cos(\omega t)). \quad (3)$$

Here, η is the parameter that decides the ellipticity of the field and is $\eta = 0(1)$ for linear(circular) polarization. Varying the η between 0 and 1 will change the ellipticity of polarization.

The time-dependent wave function, $u_{n,\mathbf{k}}(\mathbf{r}, t)$, can be expressed by Houston function,

$$w_{n,\mathbf{k}}(\mathbf{r}, t) = u_{n,\mathbf{k}+\frac{e}{c}\mathbf{A}(t)}^G(\mathbf{r}) \exp \left[-i \int^t \epsilon_{n,\mathbf{k}+\frac{e}{c}\mathbf{A}(t')}^G dt' \right], \quad (4)$$

as

$$u_{n,\mathbf{k}}(\mathbf{r}, t) = \sum_{n'} C_{nn'}^{\mathbf{k}}(t) w_{n',\mathbf{k}}(\mathbf{r}, t). \quad (5)$$

Here, $u_{n,\mathbf{k}}^G(\mathbf{r})$ is the wave function of ground state. As presented in Ref.,¹⁵⁾ we can obtain a simplified expression for the time-evolution of the coefficient $C_{nn'}^{\mathbf{k}}(t)$ as follows:

$$i \frac{\partial C_{nn'}^{\mathbf{k}}(t)}{\partial t} = i \frac{e}{mc} \frac{d\mathbf{A}(t)}{dt} \sum_{n''} C_{nn''}^{\mathbf{k}}(t) \left\langle u_{n'',\mathbf{k}+\frac{e}{c}\mathbf{A}(t)}^G \left| \frac{\partial u_{n',\mathbf{k}+\frac{e}{c}\mathbf{A}(t)}^G}{\partial \mathbf{k}} \right. \right\rangle \times \exp \left[-i \int^t dt' \Delta \epsilon_{n'',\mathbf{k}+\frac{e}{c}\mathbf{A}(t')}^G \right]. \quad (6)$$

The important quantity in Eq. (6) is the time integration of the relative energy, $\Delta \epsilon_{n'',\mathbf{k}+\frac{e}{c}\mathbf{A}(t)}^G = \epsilon_{n'',\mathbf{k}+\frac{e}{c}\mathbf{A}(t)}^G - \epsilon_{n',\mathbf{k}+\frac{e}{c}\mathbf{A}(t)}^G$, because it includes multi-photon absorption processes as discussed in following sections.

2.1 Isotropic band

In the following discussion, we assume the isotropic parabolic two-band system,

$$\epsilon_{c,\mathbf{k}}^G - \epsilon_{v,\mathbf{k}}^G = \Delta \epsilon_{cv,\mathbf{k}}^G = E_g + \frac{\hbar^2 \mathbf{k}^2}{2\mu}, \quad (7)$$

to simplify the equations and results. Here E_g is the band gap, μ is the reduced mass and the subscript c (v) corresponds to conduction (valence) band.

If we assume the transition dipole momentum to be isotropic, the transition coefficient for this model is simplified to

$$C_{vc}^{\mathbf{k}} = -\frac{ieP_{cv}A_0}{2\hbar mc} \int_{-T}^T dt [M^- e^{i\omega t} + M^+ e^{-i\omega t}] \times \exp \left[\frac{i}{\hbar} \int^t \Delta \epsilon_{cv,\mathbf{k}+\frac{e}{c}\mathbf{A}(t')}^G dt' \right] \quad (8)$$

where $M^\pm = 1 \pm i\eta$, and P_{cv} is the absolute value of the transition dipole momentum, it can be estimated as $P_{cv} \simeq m \sqrt{E_g/4\mu}$.²⁶⁾ The exponential term in Eq. (8) can be expressed as,

pressed as,

$$\exp \left[\frac{i}{\hbar} \int^t \Delta \epsilon_{cv,\mathbf{k}+\frac{e}{c}\mathbf{A}(t')}^G dt' \right] = \sum_{l,m,n} \exp \left[\frac{i}{\hbar} \left(E_g + \frac{\hbar^2 k_0^2}{2\mu} + \frac{e^2 A_0^2}{4\mu c^2} (1 + \eta^2) \right) t \right] \times J_l(\alpha) J_m(\beta) J_n(\gamma) e^{i(2l+m+n)\omega t} e^{im\frac{\pi}{2}} \quad (9)$$

where θ and ϕ are the angle of \mathbf{k} from z - and x -axis respectively, and J_i is the i -th order Bessel function with arguments:

$$\alpha = (1 - \eta^2) \frac{e^2 A_0^2}{8\hbar\mu\omega c^2} \quad (10)$$

$$\beta = \eta \frac{ek_0 A_0 \sin \theta \cos \phi}{\mu c \omega} \quad (11)$$

$$\gamma = \frac{ek_0 A_0 \sin \theta}{\mu c \omega}. \quad (12)$$

The transition rate for every \mathbf{k} is $w_{\mathbf{k}} = \lim_{T \rightarrow \infty} \frac{|C_{cv}^{\mathbf{k}}|^2}{2T}$. The total transition rate per unit time (W) is obtained by

$$W = \sum_{\mathbf{k}} w_{\mathbf{k}} = \int \frac{2k_0^2}{8\pi^3} dk_0 \sin \theta d\theta d\phi w_{\mathbf{k}} \quad (13)$$

The final expression for the transition rate is

$$W = \frac{e^2 P_{cv}^2 A_0^2 \mu^{3/2}}{4 \sqrt{2} \pi^2 \hbar^4 m^2 c^2} \sum_{L=l_0}^{\infty} \sum_{m_1, m_2} \int d\theta \sin \theta \int d\phi (-1)^{m_1-m_2} \sqrt{\kappa_L} \left[(1 + \eta^2) \left\{ J_{L-m_1-1}(\tilde{\gamma}, \tilde{\alpha}) J_{m_1}(\tilde{\beta}) J_{L+m_1-2m_2-1}(\tilde{\gamma}, \tilde{\alpha}) J_{2m_2-m_1}(\tilde{\beta}) + J_{L-m_1+1}(\tilde{\gamma}, \tilde{\alpha}) J_{m_1}(\tilde{\beta}) J_{L+m-2n+1}(\tilde{\gamma}, \tilde{\alpha}) J_{2m_2-m_1}(\tilde{\beta}) \right\} + 2(1 - \eta^2) J_{L-m_1-1}(\tilde{\gamma}, \tilde{\alpha}) J_{m_1}(\tilde{\beta}) \right. \\ \left. \times J_{L+m_1-2m_2+1}(\tilde{\gamma}, \tilde{\alpha}) J_{2m_2-m_1}(\tilde{\beta}) \right], \quad (14)$$

where $J_i(a, b)$ is the i -th order of generalized Bessel function,²⁷⁾ L is the order of multi-photon absorption, l_0 is the lowest photon process order to overcome the band gap with ponderomotive energy

$$\kappa_L = L\hbar\omega - \left\{ E_g + (1 + \eta^2) \frac{e^2 A_0^2}{4\mu c^2} \right\} \geq 0, \quad (15)$$

and the new arguments for Bessel functions ($\tilde{\alpha}, \tilde{\beta}, \tilde{\gamma}$) are

$$\tilde{\alpha} = (\eta^2 - 1) \frac{e^2 A_0^2}{8\hbar\mu\omega c^2} \quad (16)$$

$$\tilde{\beta} = \eta \frac{e \sqrt{2\kappa_L} A_0 \sin \theta \cos \phi}{\sqrt{\mu} c \omega} \quad (17)$$

$$\tilde{\gamma} = \frac{e \sqrt{2\kappa_L} A_0 \sin \theta}{\sqrt{\mu} c \omega}. \quad (18)$$

To derive Eq. (14), we impose symmetry in the integration about ϕ .

2.1.1 linear and circular polarization limit

From the definition of the ellipticity η , we can reproduce the linear and circular polarization cases as the limit of $\eta = 0$ and 1 of Eq. (14). For $\eta = 0$, the excitation rate with linearly polarized laser is

$$W = \frac{e^2 P_{cv}^2 A_0^2 \mu^{3/2}}{2 \sqrt{2} \pi \hbar^4 m^2 c^2} \times \sum_{L=l_0}^{\infty} \int d\theta \sin \theta \sqrt{\kappa_L} (J_{L+1}(\tilde{\gamma}, \tilde{\alpha}) + J_{L-1}(\tilde{\gamma}, \tilde{\alpha}))^2 \quad (19)$$

with $\tilde{\alpha} = -e^2 A_0^2 / 8 \hbar \mu \omega c^2$ and $\kappa_L = L \hbar \omega - (E_g + e^2 A_0^2 / 4 \mu c^2)$, while $\eta = 1$ gives the rate with circularly polarized laser as

$$W = \frac{e^2 P_{cv}^2 A_0^2 \mu^{3/2}}{2 \sqrt{2} \pi^2 \hbar^4 m^2 c^2} \sum_{L=l_0}^{\infty} \sum_{m_1, m_2} \int d\theta \sin \theta \int d\phi (-1)^{m_1 - m_2} \sqrt{\kappa_L} \times \left\{ J_{L-m_1-1}(\tilde{\gamma}) J_{m_1}(\tilde{\beta}) J_{L+m_1-2m_2-1}(\tilde{\gamma}) J_{2m_2-m_1}(\tilde{\beta}) + J_{L-m_1+1}(\tilde{\gamma}) J_{m_1}(\tilde{\beta}) J_{L+m_1-2m_2+1}(\tilde{\gamma}) J_{2m_2-m_1}(\tilde{\beta}) \right\}, \quad (20)$$

with $\tilde{\beta} = (ek_0 A_0 / \mu c \omega) \sin \theta \cos \phi$ and $\kappa_L = L \hbar \omega - (E_g + e^2 A_0^2 / 2 \mu c^2)$. To derive Eq. (20), we use the relation of generalized Bessel function $J_i(a, 0) = J_i(a)$. Although Eq. (19) is consistent with our previous result,¹⁵⁾ Eq. (20) is not because the definition of polarization direction is different.

2.2 Band structure dependence

In general, the reduced mass μ around the band-edge has direction dependence due to the band structure, $\mu \rightarrow \mu(\theta, \phi)$. Under the vector potential $\mathbf{A}(t)$, the momentum of electron in the Bloch phase space is changed from $\mathbf{k} = k_0(\sin \theta \cos \phi, \sin \theta \sin \phi, \cos \theta)$ to

$$\begin{aligned} \mathbf{k}'(t) &= (k_0 \sin \theta \cos \phi + \frac{e}{\hbar c} A_0 \eta \sin \omega t, \\ &k_0 \sin \theta \sin \phi, \\ &k_0 \cos \theta + \frac{e}{\hbar c} A_0 \cos \omega t) \\ &\equiv (k'_0 \sin \theta' \cos \phi', k'_0 \sin \theta' \sin \phi', k'_0 \cos \theta'). \end{aligned}$$

We have a new time-dependent Bloch wavevector with,

$$\begin{aligned} k'_0(t) &= \left(k_0^2 + \frac{e^2}{\hbar^2 c^2} A_0^2 (\cos^2 \omega t + \eta^2 \sin^2 \omega t) \right. \\ &\quad \left. + 2 \frac{e}{\hbar c} k_0 A_0 (\cos \theta \cos \omega t + \eta \sin \theta \cos \phi \sin \omega t) \right)^{1/2} \end{aligned} \quad (21)$$

$$\theta'(t) = \arccos \left[\frac{k_0 \cos \theta + \frac{e}{\hbar c} A_0 \cos \omega t}{k'_0(t)} \right] \quad (22)$$

, and

$$\phi'(t) = \arctan \left[\frac{k_0 \sin \theta \sin \phi}{k_0 \sin \theta \cos \phi + \frac{e}{\hbar c} A_0 \eta \sin \omega t} \right], \quad (23)$$

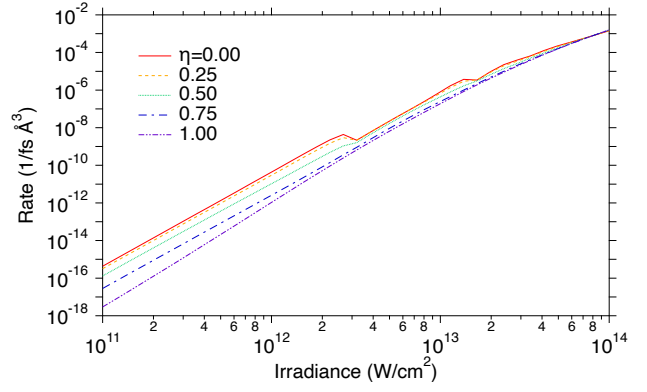


Fig. 1. Laser irradiance dependence of the excitation rate with some ellipticity (η).

we can calculate the energy phase including band structure as

$$\begin{aligned} &\exp \left[\frac{i}{\hbar} \int^t \Delta \epsilon_{cv, \mathbf{k} + \frac{e}{\hbar c} \mathbf{A}(t')} dt' \right] \\ &= \exp \left[\frac{i}{\hbar} \int^t \left(B_g + \frac{\hbar^2 \mathbf{k}_0^2}{2 \mu (\theta', \phi')^2} \right) dt' \right]. \end{aligned} \quad (24)$$

For the case of the simple M -fold symmetric system in θ and ϕ , it can be expressed as

$$\mu(\theta, \phi) = \mu_0 \left[1 + \xi \left(\sin^2 \frac{M}{2} \theta + \sin^2 \frac{M}{2} \phi \right) \right]. \quad (25)$$

The relative energy and transition dipole moment have the M -fold symmetry with the reduced mass in Eq. (25). By substituting the reduced mass to the general formula of the transition coefficient Eq (6), we can get the transition coefficient with band structure,

$$C_{vc}^{\mathbf{k}}(t) = -e \int dt' \frac{\mathbf{E}(t') \cdot \mathbf{P}_{\mathbf{k}'(t'), cv}}{E_g + \frac{\hbar \mathbf{k}'(t')^2}{2 \mu (\theta', \phi')}} \exp \left[\frac{i}{\hbar} \int dt'' \Delta \epsilon_{cv, \mathbf{k}''(t'')} \right]. \quad (26)$$

3. Results

3.1 Isotropic band

Diamond is a typical dielectric in non-linear laser-matter interaction studies, and we select it as an example to illustrate the application of the preceding formalism. The transition probability of diamond by 800 nm (1.55 eV) light is shown in Fig. 1. We assume a bandgap (B_g) of 7.4 eV and a reduced mass of 0.5 m . The lowest order of the multi-photon absorption is the 5-photon process.

The excitation rates with linear (solid red line) and circular polarization (purple double-dotted and dashed line) are same as the previous results.¹⁹⁾ The excitation rate decrease as η increases, which is consistent with the experimental results qualitatively.

The ratio of W with respect to circular polarization is shown in Fig. 2. The ratio of W accesses to one up to 7×10^{13} W/cm² for all η , while the ratio becomes less than one above 7×10^{13} W/cm². To clarify the excitation process, we plot the Keldysh parameter (γ_k) in Fig. 2 as a solid black line. In general, the tunnelling process is dominant at $\gamma_k \ll 1.0$. The reversing relationship in the ratio occurs at $\gamma_k < 0.5$, which suggests that the ellipticity dependence is different for the multi-photon and tunneling excitation processes.

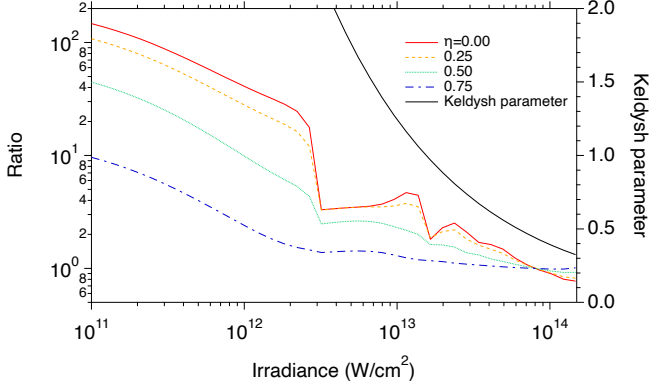


Fig. 2. Relative excitation rate with respect to circular polarization.

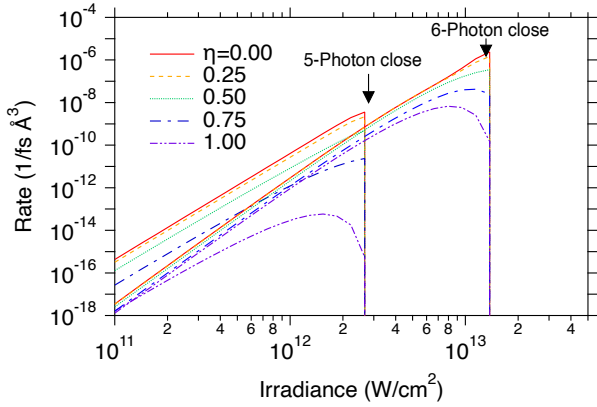


Fig. 3. Excitation rate via 5- and 6-photon processes. The abrupt drop of the rate indicates the channel closing of each photonic process.

Although linear polarization shows clear 5-photon absorption below $1 \times 10^{12} \text{ W/cm}^2$, the irradiance dependence of elliptical polarization does not. Figure 3 shows 5-photon absorption (5PA) and 6-photon absorption (6PA), which is the $L = 5$ and 6 terms of Eq. (14) respectively. The 5PA channel is closed at $2.6 \times 10^{12} \text{ W/cm}^2$, while the 6PA channel is closed at $1.4 \times 10^{13} \text{ W/cm}^2$. The 5PA rate is larger than the 6PA absorption rate with $\eta = 0.0$ and 0.25. The relationship between 5PA and 6PA is reversed as η increases because the 5PA rate decreases significantly below the channel closing with higher η . We have to consider some multi-photon processes to evaluate the excitation rate with elliptical and circular polarization.

3.2 Anisotropic band

In the previous subsection, we studied the η dependence with isotropic parabolic band. However, the η dependence is much larger than the experimental result.¹⁹⁾ In this subsection, we would like to study how the band structure affects η dependence. Since the analytical formulation with direction-dependent reduced mass like Eq. (25) is complicated, we solve Eq. (26) by real-time method.

We assume the Gaussian-shape laser pulse,

$$\mathbf{A}(t) = A_0 e^{-\frac{t^2}{\tau^2}} (\eta \sin \omega t, 0, \cos \omega t). \quad (27)$$

Since diamond has 4-fold symmetry, the reduced mass can be

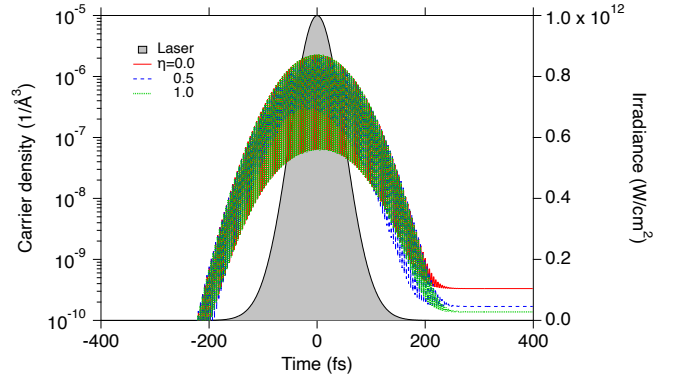


Fig. 4. Time evolution of carrier density with η as 0, 0.5, and 1.0. The grey shaded region is laser pulse irradiance. ξ is fixed at 5×10^{-3} . The solid line with grey shaded area indicates the time-evolution of the laser irradiance.

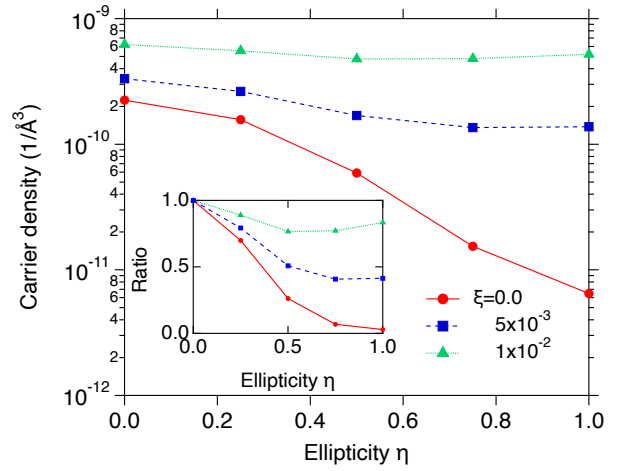


Fig. 5. Ellipticity and ξ dependence of the carrier density at the end of time evolution. The inset figure shows the carrier density scaled at $\eta = 0.0$.

mimicked by

$$\mu(\theta, \phi) = \mu_0 [1 + \xi (\sin^2 2\theta + \sin^2 2\phi)], \quad (28)$$

where ξ is the parameter for anisotropy of band structure. Figure 4 shows the time-evolution of the carrier density,

$$n(t) = \int d\mathbf{k} |\mathbf{c}_{vc}^{\mathbf{k}}(t)|^2, \quad (29)$$

with the ellipticity of 0.0, 0.5, and 1.0. The irradiance is $1 \times 10^{12} \text{ W/cm}^2$ with frequency of 1.55 eV. The pulse duration parameter τ is 100 fs. The band structure parameter, ξ , is 0.005. The isotropic band case indicates that the excitation rate with linear polarization ($\eta = 0.0$) is about 50 times higher than that with circular polarization. On the other hand, the anisotropic case indicates a factor of 2.5, which is close to the factor of 5 in experiment.¹⁹⁾

Figure 5 shows the ξ and η dependence of the carrier density. The carrier density increases at higher ξ in all η , and the η dependence decreases as the ξ increases. In particular, in the case of $\xi = 1 \times 10^{-2}$, the excitation rate has the minimum at $\eta = 0.5$. The change of η giving minimum excitation rate indicates that the band structure changes the η dependence not only quantitatively but also qualitatively.

To clarify why the excitation ξ -dependence is more intense

with higher ellipticity, we would like to revisit the phase by the time integral of the energy. If we see the electron at Γ -point with $\eta = 1.0$, the time evolution of the relative energy is

$$\Delta\epsilon_{cv,\mathbf{k}'}^G(t) = \frac{e^2 A_0^2}{\hbar^2 c^2 \mu_0} \frac{1}{1 + \xi \frac{1 - \cos 4\omega t}{2}}. \quad (30)$$

The relative energy oscillates with a frequency of 4ω . On the other hand, in the linear polarization case, the relative energy oscillates with 2ω . The higher relative energy oscillation frequency induces the increase of excitation rate. Therefore, higher η is more sensitive to ξ . Since the intra-band oscillation under elliptically polarized laser changes the η -dependence, the material with a significant anisotropic band structure may have the maximum excitation rate under circularly polarized laser.

It should be noted that ξ affects excitation rate more than we expected from the experiment.¹⁹⁾ The sensitive behavior of our model may be due to the naive treatment of the band structure. Diamond has almost isotropic band structure around the Γ -point and the direction dependence of effective mass becomes more prominent as k_0 increases. Our results indicate that the realistic band structure is essential to reproduce the experiments quantitatively.

4. Summary

We extended our previous analytical formula for the electron excitation rate in the dielectrics¹⁵⁾ to elliptical polarization. In general, ellipticity decreases the excitation rate. In particular, the ellipticity dependence is significant in the isotropic system. However, the decrease of excitation rate by elliptically polarized laser becomes small by assuming the anisotropic band structure because the symmetry-dependent oscillation of energy in the intra-band dynamics occurs with higher ellipticity. If the anisotropy of the band structure is significant, the ellipticity increases the excitation rate.

The conflict between two experimental results reported by Temnov *et. al.*²⁰⁾ and Kozák *et. al.*,¹⁹⁾ and our numerical results indicate that the anisotropy of the band structures is important to understand the laser excitation process.

5. Acknowledgment

This research is supported by MEXT Quantum Leap Flagship Program (MEXT Q-LEAP) under Grant No. JPMX0118067246. This research is also partially supported

by JST-CREST under Grant No. JP-MJCR16N5. The numerical calculations are carried out using the computer facilities of the SGI8600 at Japan Atomic Energy Agency (JAEA).

- 1) K. M. Davis, K. Miura, N. Sugimoto, and K. Hirao: Opt. Lett. **21** (1996) 1729.
- 2) K. Miura, J. Qiu, H. Inouye, T. Mitsuyu, and K. Hirao: Applied Physics Letters **71** (1997) 3329.
- 3) V. R. Bhardwaj, E. Simova, P. P. Rajeev, C. Hnatovsky, R. S. Taylor, D. M. Rayner, and P. B. Corkum: Phys. Rev. Lett. **96** (2006) 057404.
- 4) R. R. Gattass and E. Mazur: Nature Photonics **2** (2008) 219.
- 5) S. Ghimire, A. D. DiChiara, E. Sistrunk, P. Agostini, L. F. DiMauro, and D. A. Reis: Nature Physics **7** (2011) 138.
- 6) Y. S. You, D. A. Reis, and S. Ghimire: Nature Physics **13** (2017) 345.
- 7) A. Schiffrin, T. Paasch-Colberg, N. Karpowicz, V. Apalkov, D. Gerster, S. Mühlbrandt, M. Korbman, J. Reichert, M. Schultze, S. Holzner, J. V. Barth, R. Kienberger, R. Ernstorfer, V. S. Yakovlev, M. I. Stockman, and F. Krausz: Nature **493** (2013) 70.
- 8) L. Keldysh: JETP **20** (1965) 1307.
- 9) S. M. Golin, S. E. Kirkwood, D. D. Klug, D. M. Villeneuve, D. M. Rayner, C. A. T. Herrero, and P. B. Corkum: Journal of Physics B: Atomic, Molecular and Optical Physics **47** (2014) 204025.
- 10) F. H. M. Faisal: Journal of Physics B: Atomic and Molecular Physics **6** (1973) L89.
- 11) H. D. Jones and H. R. Reiss: Phys. Rev. B **16** (1977) 2466.
- 12) H. R. Reiss: Phys. Rev. A **22** (1980) 1786.
- 13) M. Ammosov, N. Delone, and V. Krainov: JETP **64** (1986).
- 14) V. E. Gruzdev: Phys. Rev. B **75** (2007) 205106.
- 15) T. Otobe, Y. Shinohara, S. A. Sato, and K. Yabana: Journal of the Physical Society of Japan **88** (2019) 024706.
- 16) T. Otobe: Phys. Rev. B **94** (2016) 165152.
- 17) A. H. Nejadmalyeri and P. R. Herman: Opt. Lett. **31** (2006) 2987.
- 18) M. Huang, F. Zhao, Y. Cheng, N. Xu, and Z. Xu: Opt. Express **16** (2008) 19354.
- 19) M. Kozák, T. Otobe, M. Zakerstein, F. Trojánek, and P. Malý: Phys. Rev. B **99** (2019) 104305.
- 20) V. V. Temnov, K. Sokolowski-Tinten, P. Zhou, A. El-Khamhawy, and D. von der Linde: Phys. Rev. Lett. **97** (2006) 237403.
- 21) T. Otobe, M. Yamagiwa, J.-I. Iwata, K. Yabana, T. Nakatsukasa, and G. F. Bertsch: Phys. Rev. B **77** (2008) 165104.
- 22) Y. Shinohara, K. Yabana, Y. Kawashita, J.-I. Iwata, T. Otobe, and G. F. Bertsch: Phys. Rev. B **82** (2010) 155110.
- 23) K. Yabana, T. Sugiyama, Y. Shinohara, T. Otobe, and G. F. Bertsch: Phys. Rev. B **85** (2012) 045134.
- 24) T. Otobe: Phys. Rev. B **96** (2017) 235115.
- 25) T. Otobe: Phys. Rev. B **94** (2016) 165152.
- 26) E. Kane: Journal of Physics and Chemistry of Solids **12** (1960) 181.
- 27) H. R. Reiss and V. P. Krainov: Journal of Physics A: Mathematical and General **36** (2003) 5575.